JOURNAL OF SPACECRAFT AND ROCKETS
Vol. 47, No. 2, March–April 2010

Formation Optimal Maneuvers Under Inertial Attitude Dynamics

Darren J. Zanon* and Mark E. Campbell†
Cornell University, Ithaca, New York 14853

DOI: 10.2514/1.44138

A technique for generating optimal maneuvers for realistic thruster placements on rotating spacecraft in formations is developed. The approach uses linear programming optimization to initialize a Hamilton–Jacobi–Bellman optimization. The linear programming solution develops a fast and accurate solution for the discretized problem; the subsequent Hamilton–Jacobi–Bellman optimization minimizes the true continuous cost (such as formation fuel use). A Schur decomposition and singular value decomposition are employed to enhance the speed and robustness of the Hamilton–Jacobi–Bellman optimization. The resultant technique scales well with the number of thruster switches and is generally applicable to spacecraft for which inertial frame dynamics are known over one or more orbits. The approach is evaluated in simulation on a two-spacecraft cooperative inspection mission. Analysis is performed on a variety of potential strategies for choosing reference centers, stabilizing relative orbits, and decreasing orbit separation distance, showing excellent performance in both solution accuracy and fuel use while reducing computation time compared with traditional approaches.

Nomenclature

$A(\theta)$	=	linear time-varying state dynamics matrix
a	=	orbit semimajor axis, km
$\mathbf{a}$	=	quaternion rotation vector
a_p	=	distance from gravitating body at perigee, km
$B(\theta)$	=	linear time-varying input matrix
C	=	constant relating time and orbit angular velocity, $a^{\frac{3}{4}}(1-e^2)^{\frac{3}{4}}\mu^{-\frac{1}{4}}$
E	=	eccentric anomaly
e	=	orbit eccentricity
$G[\omega(\theta)]$	=	gravitational linear time-varying dynamics function
h	=	base size of linear programming matrices, $m \cdot M$
$\mathcal{J}(\theta)$	=	relative drift function
J_F	=	fuel cost for arbitrary thrust set, m/s
$J_{F,u}$	=	fuel cost for orthonormal thrust set, m/s
$K(\boldsymbol{\Theta})$	=	block matrix representation of switch time constraints
M	=	number of linear programming spline segments
m	=	number of available thrusters
$\aleph$	=	linear programming thrust activation vector
$\bar{\aleph}$	=	normalized $\aleph$
$\bar{\aleph}$	=	matrix of linear programming activation elements
n_p	=	number of segments in a piecewise polynomial
$n_{p,i}$	=	number of on–off pairs for the ith thruster
n_p^*	=	total number of on–off thrust pairs
$\mathcal{O}$	=	orbits required to complete a maneuver
$\mathbf{P}$	=	relative parameterization elements for a single spacecraft $(p_1, p_2, \ldots, p_6)$, m
$\mathbf{p}_{\mathrm{PL}}$, $\mathbf{p}_{\mathrm{CR}}$	=	relative reference frame parameterization vector, planar and cross-axis components
$\mathbf{Q}$	=	vector representation of single-spacecraft thrust effect, m/s^2
$\mathcal{Q}$	=	splined thrust approximation matrix
$\mathcal{Q}_{\mathcal{S}}$	=	linear programming thrust approximation matrix
Q, D	=	matrices produced by Schur decomposition
$\mathbf{q}$	=	quaternion
$\mathbf{R}$	=	spacecraft position in inertial reference frame, m
$\mathbf{r}$	=	relative position of a spacecraft with respect to a reference orbit
$\mathcal{S}$	=	matrix of unit thrust directions, $[\mathbf{s}_1 \cdots \mathbf{s}_m]$
$T(\theta)$	=	rotation matrix from body to reference frames
t	=	time since reference perigee crossing, s
U, Σ, V	=	matrices produced by singular value decomposition
$\mathbf{u}$	=	vector thrust-to-mass ratio, m/s^2
$\mathbf{x}$	=	spacecraft state (position and velocity) in relative reference frame, m or m/s
$\mathbf{x}_p^i(\theta)$	=	relative position of ith spacecraft at true anomaly θ, m
$\mathbf{z}$	=	spacecraft state in angular velocity-normalized reference frame, m or m/s
$\boldsymbol{\alpha}(\theta)$	=	time-varying thrust activation vector (m elements)
ϵ	=	threshold value to derive on–off thrusts from linear programming solution, m/s^2
$\boldsymbol{\eta}$	=	residual vector for numerical optimization
$\boldsymbol{\Theta}$	=	set of on–off switch true anomalies
$\theta_{i,j-}$, $\theta_{i,j+}$	=	true anomalies of jth on–off thrust pair for the ith thruster
θ	=	reference-orbit true anomaly
θ_C	=	true anomaly at which formation elements are defined, rad
$\boldsymbol{\lambda}$	=	Lagrange multiplier vector
μ	=	gravitational parameter, m^3/kg-s^2
ν	=	elevation angle for relative position sphere, rad
$\boldsymbol{\xi}$	=	thruster selection matrix for linear programming
ϱ	=	separation distance for relative position sphere, m
$\rho(\theta)$	=	multiplier for orbit distance from focus, $1 + e\cos\theta$
$\Phi(\theta)$	=	fundamental matrix solution for state dynamics
ϕ	=	azimuth angle for relative position sphere, rad
$\Psi(\theta)$	=	fundamental matrix solution for costate dynamics
$\boldsymbol{\Omega}(\boldsymbol{\Theta})$	=	vector representation of switch true anomaly constraints
$\omega(\theta)$	=	spacecraft orbit angular rate
ω_n	=	orbit natural frequency
$\dot{}$	=	derivative with respect to time

Received 5 March 2009; accepted for publication 4 December 2009.

*Currently Guidance, Navigation, and Control Engineer, Comtech AeroAstro, Inc., 20145 Ashbrook Place, Ashburn, VA 20147; darren.zanon@aeroastro.com. Professional Member AIAA.

†Associate Professor, Mechanical and Aerospace Engineering, Upson Hall; mc288@cornell.edu. Associate Fellow AIAA.

Subscripts

ac	=	parameter relating to formation acquisition
st	=	parameter relating to formation stabilization

Superscripts

B	=	position or velocity in spacecraft body frame
N	=	position or velocity in inertially fixed reference frame
R	=	position or velocity in relative reference frame
$'$	=	derivative with respect to true anomaly
*	=	single spacecraft or formation optimal

I. Introduction

AUTONOMOUS satellite formations represent a means of accomplishing advanced mission objectives while reducing cost and extending mission life, and both NASA and the U.S. Department of Defense have shown interest in the continuing success of this technology [1–4]. Missions range from Earth and deep space science to space-based radar, and current defense research focuses on on-orbit docking and inspection. However, several challenges facing satellite clusters must be resolved, including fleet-wide communication, fault detection and tolerance issues, collision-avoidance methods, and effective path planning and control in the presence of disturbances. This paper focuses on the last of these concerns by presenting a problem-solving methodology that can be applied to a wide range of planning and control scenarios.

Planning and control are often partitioned into two distinct modes, though the dynamics employed are typically similar, if not identical [5]. Formation maneuvering is considered the moving of the cluster of spacecraft from one desired formation to another. Formation keeping is a mode in which the spacecraft are controlled to remain in their current formation to within a specified tolerance in the presence of disturbances. Each of these problems must be fully understood (and the systems properly integrated) if autonomous satellite formations are to succeed in future missions. This paper addresses formation keeping when attitude constraints are present, which is a problem of particular relevance to inspection and docking missions [6].

Both formation keeping and close formation maneuvering rely on dynamics expressed in a linearized relative reference frame. A review of both theoretical and practical solutions and applications for a single spacecraft in this frame is given in [7,8]. However, higher-order orbit descriptions [9,10] and alternative linearizations [11] have also been used in some applications. One technique for controlling motion in the relative frame is the convex optimization approach developed by Tillerson et al. [5,12] in which the trajectory is discretized with true anomaly and a linear programming (LP) method is employed to generate an optimal trajectory; this discretization can be applied to both formation keeping and formation maneuvering [13]. Because of constraints on the problem formulation, however, the LP method can be computationally intensive for long-term or highly constrained problems. Hamilton–Jacobi–Bellman (HJB) optimality conditions have also been successfully used to develop time- and fuel-optimal maneuvers in the relative reference frame [13,14]. This method guarantees that necessary conditions for optimality are satisfied and is most useful for solving problems in the relative reference frame about eccentric orbits when the optimization algorithm is initialized in the neighborhood of the optimal solution.

Algorithms for formation maneuvering using either of these methods have typically required the assumption that thrust can be generated in any direction [15,16]. Planning methodologies with attitude constraints have been developed for systems near Lagrange points [17,18], where slower, symmetric dynamics can be used advantageously. These techniques do not readily apply to the highly eccentric orbits demanded by missions such as Magnetospheric Multiscale [1]. One approach to circumventing this issue is to control thruster pointing during the maneuver, which was recently explored by Hall and Ross [19]. This method is largely intended for long-duration, minimum-time maneuvers with constant thrust and does not work well for spin-stabilized spacecraft or those in close proximity.

Formation maneuvering with attitude dynamics is closely associated with autonomous rendezvous and docking, which has a long history in the literature [20–22]. Much work on these missions has focused on vision systems, thruster control techniques, or mode switching and power allotment [23–25]. Some control and planning alternatives have also been explored that seek to limit fuel use in the presence of path constraints, but body dynamics are simplified in the interests of computability [26].

This paper explores a realistic formation-maneuvering problem in which a spacecraft has multiple thrusters and undergoes attitude variations that are dynamically significant and predictable during maneuvering. For most small spacecraft, available thrust is confined to specific directions and is subject to the kinematics of the spacecraft body. This paper develops a novel technique for formation maneuvering with attitude constraints by implementing a mixed linear programming/Hamilton–Jacobi–Bellman optimization scheme that uses a paired Schur decomposition and singular value decomposition to generate near-optimal maneuvers in the relative reference frame. This technique uses the benefits of both planning methodologies: namely, the initializability of the LP method and the optimality and scalability of the HJB method. The approach can be applied to formations by including both spacecraft among the constraints, and a variety of problems can be probed that maximize mission life and effectiveness. The algorithm developed here is parallelizable across a cluster and scalable to larger problems, including those spanning multiple orbits. Unlike LP alone, the computation time of the mixed LP-M/HJB algorithm is approximately constant for a large class of problems, and the solution is not subject to discretization errors. Also, in contrast to the separate HJB formulation, initialization is easier, such that a nearby solution that best satisfies state and costate constraints will nearly always be found, often in less time than using standard initializations of HJB.

Testing of this approach is performed on problems specific to the requirements of a proposed inspection mission in which attitude constraints are an important component. Sponsored by the U.S. Air Force Research Laboratory, the Cornell University NanoSat (CU Sat) project is a two-spacecraft inspection mission that demands both formation acquisition and long-term formation maintenance, as well as a variety of on-orbit maneuvers [27]. The spacecraft are spin-stabilized and typically operate within 50 m of one another. Accessibility and testing of the technologies required for the completion of the CU Sat mission has been highly scrutinized in recent literature [6,28], and CU Sat offers an opportunity to perform on-orbit verification of several autonomous systems, including formation-maneuvering algorithms.

The work is presented in three parts. Section II introduces the formation-maneuvering problem with attitude constraints and describes the dynamics necessary to generate near-optimal maneuvers in both HJB and LP formulations. Section III discusses both the Hamilton–Jacobi–Bellman and linear programming techniques, illustrating their application and advantages and disadvantages for use on the problem at hand. This section then describes the mixed formulation that can be used to solve problems in a way that takes advantage of the best properties of each. In Sec. IV, the specifications of the CU Sat mission are discussed. The combined technique is then employed on a variety of examples that relate to this mission.

II. Problem Definition

Consider a spacecraft undergoing relative motion with respect to a reference orbit that is subject to the dynamics of a gravitational field. Additionally, suppose this spacecraft has a finite number of thrusters that are fixed on the spacecraft body but not with respect to the inertial frame. The purpose of this work is to efficiently determine a fuel-optimal maneuvering strategy for moving this spacecraft between two points in the relative reference frame.

The need for attitude constraints is inherent in the notion of thrusters whose positions are time-dependent. To solve this problem, three elements must be considered: 1) gravitational dynamics of the spacecraft in the relative reference frame, 2) rotational dynamics of the body frame with respect to the relative reference frame, and 3) planning strategies typically using optimization tools. This paper primarily focuses on the first and third of these elements while assuming that the spacecraft undergoes a prescribed rotation. However, the methods described are flexible enough to incorporate any variety of time-dependent spacecraft motion. The addition of torque effects by the thrusters on the spacecraft body rotation creates a significantly more complex problem that the current formulation can handle, but with an added computational expense.

A. Relative Dynamics

Determination of optimal planning maneuvers with attitude constraints depends on a description of the spacecraft's state in proximity to a known elliptical reference orbit. The dynamics governing a body in motion near such an orbit are given in [29–31]. Generally, the equations of motion for a satellite with thrust-to-mass ratio $\mathbf{u}$ near a reference orbit that is in a general force field $f(\mathbf{R})$ are given by

$$\ddot{\mathbf{r}} = -f(\mathbf{R})\mathbf{r} - f'(\mathbf{R})\left(\frac{\mathbf{R}\cdot\mathbf{r}}{|\mathbf{R}|}\right)\mathbf{R} + \mathbf{u} \tag{1}$$

where $\mathbf{R} \in \mathbb{R}^{3\times 1}$ is the position of a reference satellite with respect to the gravitational body and $\mathbf{r} \in \mathbb{R}^{3\times 1}$ is the relative position of the spacecraft from this reference, such that $|\mathbf{r}| \ll |\mathbf{R}|$.

Transforming via the angular velocity of the reference orbit, the relative dynamics can be linearized as a function of the reference-orbit true anomaly θ rather than time. Humi [31] introduces the transformed coordinate $\mathbf{z}(\theta) = [\,y_1 \quad v_1 \quad y_2 \quad v_2 \quad y_3 \quad v_3\,]^T$ and shows

$$\mathbf{z}'(\theta) = \begin{bmatrix} 0 & 1 & 0 & 0 & 0 & 0 \\ 0 & 0 & 0 & 2 & 0 & 0 \\ 0 & 0 & 0 & 1 & 0 & 0 \\ 0 & -2 & G[\omega(\theta)] & 0 & 0 & 0 \\ 0 & 0 & 0 & 0 & 0 & 1 \\ 0 & 0 & 0 & 0 & -1 & 0 \end{bmatrix}\mathbf{z}(\theta) + \omega(\theta)^{-\frac{3}{2}}\begin{bmatrix} 0 & 0 & 0 \\ 1 & 0 & 0 \\ 0 & 0 & 0 \\ 0 & 1 & 0 \\ 0 & 0 & 0 \\ 0 & 0 & 1 \end{bmatrix}\mathbf{u}(\theta) \tag{2}$$

where

$$G[\omega(\theta)] = -\frac{\mathrm{d}}{\mathrm{d}R}\left(\frac{\mu}{R(\theta)^3}\right)\frac{R(\theta)}{\omega(\theta)^2}$$

and prime denotes differentiation with respect to true anomaly. This is a linear system that can be written

$$\mathbf{z}'(\theta) = A(\theta)\mathbf{z}(\theta) + B(\theta)\mathbf{u}(\theta) \tag{3}$$

The solution to this linear system is

$$\mathbf{z}(\theta) = \Phi(\theta)\Phi^{-1}(\theta_0)\mathbf{z}(\theta_0) + \Phi(\theta)\mathbf{Q}[\theta_0, \theta] \tag{4}$$

Closed-form solutions for the fundamental matrix solution $\Phi(\theta)$ and its inverse are as given by Carter [32]. The vector $\mathbf{Q}[\theta_0, \theta]$ is the thrust effect vector

$$\mathbf{Q}[\theta_0, \theta] = \int_{\theta_0}^{\theta} \Phi^{-1}(\tau)B(\tau)\mathbf{u}\,\mathrm{d}\tau \tag{5}$$

and can be solved in closed-form as given by Zanon and Campbell [13]. This solution is valid for eccentricities $0 \le e < 1$, though its precision falls off as $e \to 1$.

The system can be described in the relative reference frame by

$$x_1(\theta) = \frac{p_1}{\rho(\theta)} + \left(\frac{1}{\rho(\theta)} + 1\right)(ep_2\cos\theta + p_3\sin\theta) + p_4[2e\mathcal{J}(\theta)\rho(\theta)] \tag{6}$$

$$x_2(\theta) = p_3\cos\theta - ep_2\sin\theta - p_4\left[\frac{e\cos\theta}{\rho(\theta)^2} - 2e^2\mathcal{J}(\theta)\right] \tag{7}$$

$$x_3(\theta) = p_5\frac{\sin\theta}{\rho(\theta)} + p_6\frac{\cos\theta}{\rho(\theta)} \tag{8}$$

where $\rho(\theta) = 1 + e\cos\theta$ and

$$\mathcal{J}(\theta) = \frac{\sin\theta}{\rho(\theta)} - 3e(1-e^2)^{-\frac{5}{2}}\left[\frac{E}{2} - \frac{1}{2}\sin E\cos E - \frac{e}{3}\sin E^3\right] \tag{9}$$

with E the eccentric anomaly. In angular velocity-weighted $\mathbf{z}$ coordinates, where $\mathbf{y} = \omega(\theta)^{\frac{1}{2}}\mathbf{x}(\theta)$, and using $\omega(\theta) = \rho(\theta)^2/C^2$, this can be written simply in terms of the fundamental matrix solution:

$$\mathbf{z}(\theta) = \Phi(\theta)C^{-1}\begin{bmatrix}\begin{bmatrix} -ep_2 \\ -p_3 \\ p_4 - ep_3 \\ p_1 \end{bmatrix} \\ \begin{bmatrix} p_6 \\ p_5 \end{bmatrix}\end{bmatrix} = \Phi(\theta)C^{-1}\begin{bmatrix}[\mathbf{p}_{\mathrm{PL}}] \\ [\mathbf{p}_{\mathrm{CR}}]\end{bmatrix} \tag{10}$$

The relative frame definition shows the effect of parameter p_1, which gives the planar center of the motion; the pair (p_2, p_3) defines the boundaries of an ellipse with approximate radius $\sqrt{p_3^2 + (ep_2)^2}$. The cross-axis pair (p_5, p_6) defines displacements at apogee and perigee. Figure 1 illustrates these formation parameter definitions in the relative reference frame $\mathbf{x}^R$. A *stable orbit* is defined as one for which $\mathbf{z}(\theta) = \mathbf{z}(\theta + 2\pi)$ for all true anomalies θ. For these orbits, the sixth parameter p_4, which defines the instability of the system, is identically 0. For unstable orbits, p_4 may take any value.

B. Satellite Rotations

The gravitational dynamics relative to a reference orbit outlined in the previous section are sufficient to describe the state of the origin of

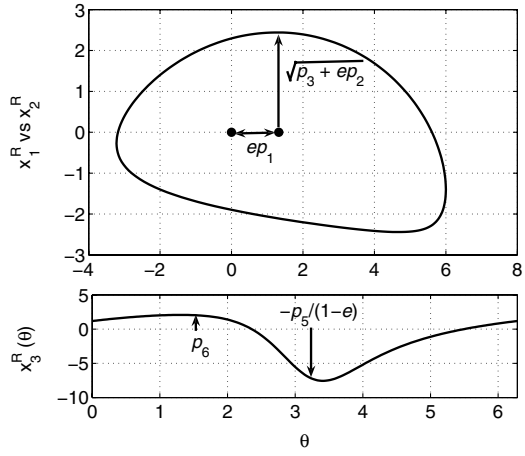

Fig. 1 Conceptual definitions of the stable parameter set P as they relate to relative reference true anomaly θ.

a body-axis coordinate frame, but they do not capture the motion of the axes themselves. In particular, most optimal planners do not account for spacecraft rotations that affect the magnitude and direction of the thrust effects. Because these are bound to the internal dynamics of the spacecraft, it is necessary to incorporate them into the planning methodology.

Consider a spacecraft as shown in Fig. 2. The spacecraft position is defined about a gravitational center as $\mathbf{x}^N$, or in proximity to a reference orbit as $\mathbf{x}^R$. The spacecraft has m discrete thrusters with maximum thrust-to-mass output $u_{\max}$ that are located independently of the relative reference axes and fixed in the body frame with directions $\mathbf{x}^B_{1-m}$; the body axes are further assumed to exhibit some form of rotational motion with respect to the relative coordinate frame, and this rotation is presumed to be known a priori. Practically, this typically means that a separate controller is used to maintain a specified attitude or rotation rate, which is a common occurrence. In this case, the 3×1 thrust vector $\mathbf{u}(\theta)$ is written as

$$\mathbf{u}(\theta) = T(\theta)\mathcal{S}\boldsymbol{\alpha}(\theta) \tag{11}$$

where the $3 \times m$ matrix $\mathcal{S}$ is the body-frame direction of the applied force from each thruster:

$$\mathcal{S} = [\, s_1 \quad s_2 \quad \ldots \quad s_m \,] \tag{12}$$

The $m \times 1$ vector $\boldsymbol{\alpha}$ then indicates that the thrust applied by each thruster, bounded by $[0, |u_{\max}|]$. The matrix $T(\theta) \in \mathbb{R}^{3\times3}$ is a three-axis rotation matrix defining the orientation of the spacecraft body with respect to the linearized reference coordinate frame. If T is only known as a function of time, the relation with true anomaly is found through

$$\omega_n t = E - e \sin E \tag{13}$$

$$\cos E = \frac{\cos\theta + e}{1 + e\cos\theta} \qquad \sin E = \frac{\sqrt{1-e^2}\sin\theta}{1 + e\cos\theta} \tag{14}$$

where ω_n is the reference-orbit mean motion or natural frequency, e is the reference eccentricity, and E is the eccentric anomaly of the reference orbit.

Because of the time-varying nature of the matrix $T(\theta)$, the thrust integral $\mathbf{Q}$ in Eq. (4) cannot, in general, be computed in closed form. However, as shown in [14], an approximation of the integrands can be defined using a piecewise polynomial spline to approximate the integrand of the thrust effect integral. Because polynomials are readily integrated, a sufficiently good approximation to this integrand yields a good approximation to the integral itself. For the purposes of this discussion, $\boldsymbol{\alpha}(\theta)$ is assumed to be piecewise constant, such that the unmultiplied spline integral becomes

$$\mathcal{Q}[\theta_{j-}, \theta_{j+}] \approx \int_{\theta_{j-}}^{\theta_{j+}} \Phi^{-1}(\theta)B(\theta)T(\theta)\,\mathrm{d}\theta \tag{15}$$

This is a 6×3 matrix for which the actual thrust effect over some interval $[\theta_1, \theta_2]$ is found by

$$\mathbf{Q}[\theta_{j-}, \theta_{j+}] = \mathcal{Q}[\theta_{j-}, \theta_{j+}]\mathcal{S}\boldsymbol{\alpha}_j \tag{16}$$

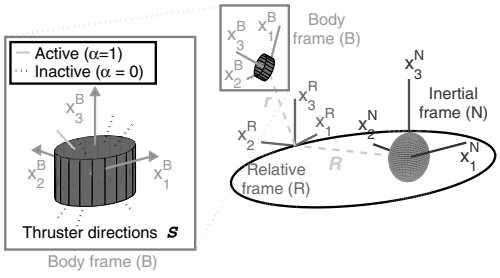

Fig. 2 Relevant coordinate frames for the problem definition.

For $T(\theta) = I$, which corresponds to axial thruster pointing, $\mathcal{Q}$ can be found in closed form using the equations derived in [13]. Comparative studies of this closed-form result with those given by spline approximations show that a piecewise polynomial using 256 intermediate points yields a solution accurate to $\lesssim 10^{-5}$ m in final position error for planning on maneuvers traversing 100 m in one orbit at eccentricities of $e = 0.8$. A complete discussion of the properties of spline interpolations can be found in [33,34].

If the time-varying function $\boldsymbol{\alpha}(\theta)$ is taken to be piecewise constant with n_p segments, the state equation can then be recast in a more general form as

$$\mathbf{z}(\theta) = \Phi(\theta)\Phi^{-1}(\theta_0)\mathbf{z}(\theta_0) + \Phi(\theta)\sum_{j=1}^{n_p} \mathcal{Q}[\theta_{j-}, \theta_{j+}]\mathcal{S}\boldsymbol{\alpha}_j \tag{17}$$

This corresponds to a series of thrust applications in which all time dependencies are resolved in the spline integral $\mathcal{Q}$. Further specifying this as a set of switches performed by each thruster, the state equation becomes

$$\mathbf{z}(\theta) = \Phi(\theta)\Phi^{-1}(\theta_0)\mathbf{z}(\theta_0) + \Phi(\theta)\sum_{i=1}^{m}\sum_{j=1}^{n_{p,i}} \mathcal{Q}[\theta_{i,j-}, \theta_{i,j+}]\mathbf{s}_i\boldsymbol{\alpha}_{i,j} \tag{18}$$

where $\mathbf{s}_i$ is the ith column of $\mathcal{S}$ and gives the body-frame position of the ith thruster. Note that n_p is potentially different for each thruster, as each thruster switches independently of the others. The spline integral $\mathcal{Q}$ can also be generated for any time-varying attitude over any number of orbits.

III. Fuel-Optimal Planners with Attitude Constraints

Minimizing fuel cost is appropriate during both formation maneuvering and formation keeping. The minimum fuel cost function is generally given as

$$J_{F,u} = \int_{\theta_0}^{\theta_F} |\mathbf{u}(\theta)|\omega(\theta)^{-1}\,\mathrm{d}\theta \tag{19}$$

with $\omega(\theta)$ relating the time and true anomaly differentials:

$$\mathrm{d}t = \sqrt{\frac{a^3}{\mu}}\frac{(1-e^2)^{\frac{3}{2}}}{2}\,\mathrm{d}\theta = \omega(\theta)^{-1}\,\mathrm{d}\theta \tag{20}$$

When multiple thrusters whose positions are not fixed in the relative reference frame are available, this may not capture the desired cost for a maneuver. The more general cost function considered here is

$$J_F = \int_{\theta_0}^{\theta_F} |\boldsymbol{\alpha}(\theta)|\omega(\theta)^{-1}\,\mathrm{d}\theta \tag{21}$$

with $\boldsymbol{\alpha}(\theta)$ defined in Eq. (11). In the case in which no active thruster generates a force along any axis that opposes that generated by any other active thruster along that axis, Eq. (21) reduces to Eq. (19).

Solving for thrust profiles using this cost function allows several solution approaches. One method assumes a thrust profile and solves using Hamilton–Jacobi–Bellman (HJB) optimality conditions. This technique has the advantage of finding the locally optimal point (and often a globally optimal point) if the optimization converges; it also scales well with maneuver type, including variations in thruster performance, eccentricity, number of spacecraft, and available thrust [14]. The primary disadvantage of HJB, however, is that a poor initial guess will often lead to convergence to a point that is not globally optimal; this becomes an issue for more complex maneuvers such as those proposed here with attitude constraints. A second method for solving minimum-fuel problems discretizes the temporal space and solves for the thrust using an LP technique [12,35]. The LP method easily incorporates inequality and equality constraints, and advances in LP solvers have led to relatively speedy solution times for a large class of problems. However, the method does not scale well

computationally, particularly as more points are added to account for maneuver length, eccentricity, and thruster performance or as the number of available thrusters and spacecraft increases.

Proposed here is the development of a formation planning methodology that integrates the HJB and LP solution techniques into a more useful solver that retains most of the advantages of each, with few of the disadvantages. The proposed mixed LP-*M*/HJB solution approach scales better computationally than LP while retaining its allowances for equality and inequality constraints. The proposed mixed LP-*M*/HJB algorithm also retains the optimality guarantees of HJB while providing an effective initialization. The remainder of this section presents the LP and HJB planner solutions, followed by the unique mixed LP-*M*/HJB planning methodology.

A. Hamilton–Jacobi–Bellman Optimization

Similar to the optimal planner developed by Zanon and Campbell [14], the Hamilton–Jacobi–Bellman solutions considered here assume bang–off–bang thrust, beginning at true anomaly θ_0 and ending at true anomaly θ_F. This constraint also exists inherently in many applications such as CU Sat, which uses pulsed-plasma thrusters (PPTs) incapable of partial thrusting [36]. The optimal Hamilton–Jacobi–Bellman method begins by augmenting the cost function given in Eq. (21) with the dynamics and thrust definitions using Lagrange multipliers:

$$J_F = \int_\theta (|\boldsymbol{\alpha}(\theta)|\omega(\theta)^{-1} + \boldsymbol{\lambda}_1(\theta)^T[\mathbf{z}'(\theta) - A(\theta)\mathbf{z}(\theta) - B(\theta)\mathbf{u}(\theta)] + \boldsymbol{\lambda}_2(\theta)^T[\mathbf{u}(\theta) - T(\theta)\mathcal{S}\boldsymbol{\alpha}(\theta)])\,\mathrm{d}\theta \tag{22}$$

Taking the variation with respect to both $\boldsymbol{\alpha}$ and $\mathbf{u}$ yields the following necessary conditions:

$$\boldsymbol{\lambda}_2^T(\theta) = \boldsymbol{\lambda}_1^T(\theta)B(\theta) \quad \forall\ \theta \tag{23}$$

$$\boldsymbol{\lambda}_1'(\theta) = -A^T(\theta)\boldsymbol{\lambda}_1(\theta) \quad \forall\ \theta \tag{24}$$

$$\boldsymbol{\lambda}_2^T(\theta)T(\theta)\mathbf{s}_i = -\omega(\theta)^{-1} \quad \forall\ \theta = \{\theta^*_{i,j-}, \theta^*_{i,j+}\} \tag{25}$$

where i is the index of the switching thruster, $\theta^*_{i,j-}$ represents the true anomaly at which the jth segment of the ith thruster begins, and $\theta^*_{i,j+}$ is the true anomaly at which this segment ends. As before, $\mathbf{s}_i$ is the body-frame direction vector associated with that thruster. Note that the same condition must be satisfied when the thruster turns on or off, which means that these conditions are not sufficient for optimality. However, Eq. (25) need not be satisfied at the endpoints $\theta = \{\theta_0, \theta_F\}$ of the period in which the maneuver occurs. The series of switches must also result in the desired final state from Eq. (18). Solving Eqs. (23–25) for $\boldsymbol{\lambda}_1$ and setting $\boldsymbol{\lambda} = \boldsymbol{\lambda}_1$, this reduces to

$$\boldsymbol{\lambda}'(\theta) = -A^T(\theta)\boldsymbol{\lambda}(\theta) \quad \forall\ \theta \tag{26}$$

$$\boldsymbol{\lambda}^T(\theta)B(\theta)T(\theta)|u_{\max,i}|s_i = -\omega(\theta)^{-1} \quad \forall\ \theta = \{\theta^*_{i,j-}, \theta^*_{i,j+}\} \tag{27}$$

Solving Eq. (26), the value of $\boldsymbol{\lambda}(\theta)$ at any true anomaly is related to the initial value of $\boldsymbol{\lambda}_0$ by

$$\boldsymbol{\lambda}(\theta) = \Psi(\theta)\Psi^{-1}(\theta_0)\boldsymbol{\lambda}_0 \tag{28}$$

with $\Psi(\theta)$ and its inverse as given by Carter [32], and $\boldsymbol{\lambda}(\theta) \in \mathbb{R}^{6\times 1}$.

For a maneuver with

$$n_p^s = \sum_{i=1}^{m} n_{p,i}$$

switches, the switching relations from Eq. (27) can be written in compact matrix form as

$$K(\theta^*_{1,1-}, \theta^*_{1,1+}, \ldots, \theta^*_{m,n_{p,m}-}, \theta^*_{m,n_{p,m}+})\boldsymbol{\lambda}_0 = \boldsymbol{\Omega}(\theta^*_{1,1-}, \theta^*_{1,1+}, \ldots, \theta^*_{m,n_{p,m}-}, \theta^*_{m,n_{p,m}+}) \tag{29}$$

where K is then an $2n_p^s \times 6$ matrix and $\boldsymbol{\Omega}$ is a column vector with $2n_p^s$ elements. Each set of $2n_{p,i}$ block rows of this matrix relation is associated with the switches for one thruster. The jth row of the ith block of the matrix K is given by two rows:

$$K_{i,j} = \begin{bmatrix} \mathbf{s}_i^T T^T(\theta^*_{i,j-})B^T(\theta^*_{i,j-})\Psi^T(\theta^*_{i,j-})\Psi^{-T}(\theta_0) \\ \mathbf{s}_i^T T^T(\theta^*_{i,j+})B^T(\theta^*_{i,j+})\Psi^T(\theta^*_{i,j+})\Psi^{-T}(\theta_0) \end{bmatrix} |u_{\max,i}| \tag{30}$$

Likewise, the jth element of $\boldsymbol{\Omega}$ associated with the block belonging to the ith thruster is the pair

$$\boldsymbol{\Omega}_{i,j} = [-\omega(\theta^*_{i,j-})^{-1}, -\omega(\theta^*_{i,j+})^{-1}]^T$$

If either $\theta^*_{i,j-} = \theta_0$ or $\theta^*_{i,j+} = \theta_F$, the corresponding row of K may be set to six zeros, along with the proper element of $\boldsymbol{\Omega}$.

For maneuvers that last less than one orbit in length and for which $T(\theta) = I$ and $n_p^s \le 6$ [14,37]. In general, however, $n_p^s > 6$, resulting in an overdetermined system that must be solved numerically. The solutions presented here use the Schur decomposition to find a numerically stable value for the vector $\boldsymbol{\lambda}_0$, then compute a singular value decomposition to isolate the linearly independent rows and ensure the costate equations are satisfied to desired precision.

For the remainder of this discussion, dependence of K and Ω on the switch times $\boldsymbol{\Theta} = \{\theta^*_{1,1-}, \ldots, \theta^*_{m,n_{p,m}+}\}$ is implied for the sake of simplicity. premultiplying Eq. (29) by K^T results in

$$K^T K\boldsymbol{\lambda}_0 = K^T\boldsymbol{\Omega} \tag{31}$$

Taking a Schur decomposition of the matrix $K^T K$ results in orthonormal matrix $Q \in \mathbb{R}^{6\times 6}$ and diagonal matrix $D \in \mathbb{R}^{6\times 6}$ such that

$$QDQ^T\boldsymbol{\lambda}_0 = K^T\boldsymbol{\Omega} \tag{32}$$

This is similar to finding a pseudoinverse of $K^T K$, but the diagonal D holds on the eigenvalues of the system. This is then inverted to solve for $\boldsymbol{\lambda}_0$:

$$\boldsymbol{\lambda}_0 = QD^{-1}Q^T K^T\boldsymbol{\Omega} \tag{33}$$

This is useful for iterative solving of the costate equation for a $\boldsymbol{\lambda}_0$ while satisfying the constraints, because, as shown by Hoffman and Wielandt [38], if the matrix K varies by a small amount, the variation in eigenvalues in D found through the Schur decomposition will be bounded by $\|K\|^2$. Even when the matrix D is nearly singular, this limits the variations in the value of $\boldsymbol{\lambda}_0$ for successive steps in an iterative solver, allowing numerically stable calculation of a Jacobian and Hessian.

The value determined for $\boldsymbol{\lambda}_0$ [Eq. (33)] using a Schur factorization can then be used to solve for the switch true anomalies in Eq. (29). Performing a singular value decomposition on the left-hand side of Eq. (29) yields

$$U\Sigma V^T\boldsymbol{\lambda}_0 = \boldsymbol{\Omega} \tag{34}$$

where $U \in \mathbb{R}^{2n_p^s \times 2n_p^s}$ and $V \in \mathbb{R}^{6\times 6}$ are orthonormal matrices and $\Sigma \in \mathbb{R}^{2n_p^s \times 6}$ holds the six singular values of the matrix K along its top diagonal. Substituting the initial condition of the costate based on the Schur decomposition, multiplying by U^T, and collecting the terms yields

$$\Sigma V^T QD^{-1}Q^T K^T\boldsymbol{\Omega} = U^T\boldsymbol{\Omega} \tag{35}$$

The matrix D must be invertible in this equation. If it is not, the HJB solution does not have six linearly independent relations, and the vector $\boldsymbol{\lambda}_0$ is much harder to determine or does not exist.

In an iterative solver, the objective is to satisfy Eq. (35) to within numerical precision. The kth step of the iteration results in a residual vector $\boldsymbol{\eta}_k$, such that

$$(\Sigma_k V_k^T Q_k D_k^{-1} Q_k^T K_k^T - U_k^T)\boldsymbol{\Omega}_k = \boldsymbol{\eta}_k \tag{36}$$

This formulation can be used in any optimization procedure in which an input vector $\boldsymbol{\Theta}$ is used to drive the residual vector $\boldsymbol{\eta} \to 0$. As long as D_k is invertible, the computed value of $\boldsymbol{\lambda}_{0,k}$ varies continuously for small changes in the set of switch true anomalies $\boldsymbol{\Theta}$. This property aids (but does not guarantee) convergence to the optimal true anomaly set $\boldsymbol{\Theta}^*$ in most off-the-shelf solvers.

B. Linear Programming Optimization

The optimal LP approach first discretizes the control input with M segments over true anomalies $\{\theta_1, \theta_2, \ldots, \theta_M\}$. Stacking control segments from m thrusters at each of the M true anomalies yields a vector of length $h = m \cdot M$. This is represented as

$$\boldsymbol{\aleph} = [\,\boldsymbol{\alpha}(\theta_1)^T \quad \boldsymbol{\alpha}(\theta_2)^T \quad \cdots \quad \boldsymbol{\alpha}(\theta_M)^T\,]^T \in \mathbb{R}^{h\times 1} \tag{37}$$

Assuming that each discrete segment is of temporal width Δt, the fuel cost function from Eq. (21) can be approximated as

$$J_F \approx \boldsymbol{\xi}^T \boldsymbol{\aleph} \Delta t \tag{38}$$

where $\boldsymbol{\xi} \in \mathbb{R}^{h\times 1}$ is a selection matrix between the m thrusters at all time steps defined such that

$$\boldsymbol{\xi}\,(i) \in [0, 1] \quad \forall\ i \in [1, \ldots, h]$$

For each discrete segment in time, an associated thrust effect integral $\mathcal{Q}[\theta_{j-}, \theta_{j+}]$ can be calculated according to Eq. (15). To accommodate nonaxial thrusters, this integral must be multiplied by the matrix $\mathcal{S}$ to obtain the thrust that can be generated by each thruster over the given interval. The total thrust effect is then given by $\mathcal{Q}_{\mathcal{S}} \in \mathbb{R}^{6\times h}$ as

$$\mathcal{Q}_{\mathcal{S}} = [\,\mathcal{Q}[\theta_0, \theta_1]\mathcal{S} \quad \mathcal{Q}[\theta_1, \theta_2]\mathcal{S} \quad \ldots \quad \mathcal{Q}[\theta_{M-1}, \theta_F]\mathcal{S}\,] \tag{39}$$

Because spacecraft typically operate with all thrusters capable of equal output, each thruster is assumed to have the same maximum available thrust, such that $|u_{\max,i}| = |u_{\max}|$. The thruster vector is then normalized as $\bar{\boldsymbol{\aleph}} = \boldsymbol{\aleph}/|u_{\max}|$, and the LP optimization problem can be cast as

$$\min_{\bar{\boldsymbol{\aleph}}} \boldsymbol{\xi}^T \bar{\boldsymbol{\aleph}} \tag{40}$$

subject to the constraints

$$\mathcal{Q}_{\mathcal{S}} \bar{\boldsymbol{\aleph}} = \Phi(\theta_F)^{-1}\mathbf{z}(\theta_F) - \Phi(\theta_0)^{-1}\mathbf{z}(\theta_0) \tag{41}$$

$$\begin{bmatrix} I_{h\times h} \\ -I_{h\times h} \end{bmatrix} \bar{\boldsymbol{\aleph}} \le \begin{bmatrix} \mathbf{1}_{h\times 1} \\ \mathbf{0}_{h\times 1} \end{bmatrix} \tag{42}$$

The constraint in Eq. (41) requires the dynamics from Eq. (18), and the constraint in Eq. (42) enforces the bounded piecewise-constant nature of the thrusts.

As shorthand for comparison and use, the LP with M discretization points will be referred to as LP-M. The proposed LP method assumes that the control thrusts are bounded rather than on–off thrust, such that elements of $\bar{\boldsymbol{\aleph}}$ may take any value in the closed interval from 0 to 1. Formulating the problem using mixed-integer linear programming allows enforcement of the on–off condition, but at the expense of computation. For small thrust limits and long maneuver times, the bounded LP provides a good approximation of the solution, and a thresholding function can be used to ensure that thrusts are simply 0 or 1. This is appropriate here because the LP is used to provide an initial guess for the HJB solver, which then refines the switch times to provide a near-optimal thrust profile. Numerically, a typical choice is to enforce the restriction:

$$\begin{aligned} \bar{\boldsymbol{\aleph}}_i &= 1 \quad \text{if } \boldsymbol{\aleph}_i > \epsilon \\ \bar{\boldsymbol{\aleph}}_i &= 0 \quad \text{otherwise} \end{aligned} \tag{43}$$

This construction is useful for converting thrusts obtained using the LP technique into switch true anomalies that can be used as an initialization for the mixed LP-M/HJB technique introduced in Sec. III.B.

To summarize, an LP solution is found by discretizing the time window into M segments, then stacking the thrust vector $\boldsymbol{\alpha}$ associated with each segment into the larger vector $\bar{\boldsymbol{\aleph}}$. The potential thrust effect for each segment is given by the matrix $\mathcal{Q}_{\mathcal{S}}$. The LP then solves the resultant problem with both constraints on the state equality and the available thrust inequality. The final solution vector is then thresholded to construct a feasible space of vectors in which thrusters are either on or off. This provides a near-optimal solution to the fuel-optimal on–off thruster problem, yielding accurate solutions without requiring a high level of computation. This problem can be solved identically over one or multiple orbits, though solution precision declines as the number of orbits increases.

C. Integrated LP-M/HJB Algorithm Realization

Solving the HJB and LP problems can easily be accomplished by encoding the problem into a compact form for use with standard solving methods, such as those provided in MATLAB or other off-the-shelf software. As noted, the computation time and memory of the LP solver scales as the number of true anomaly points M and the number of thrusters m increases. However, a variety of tools exist that allow this problem to be solved for less memory-intensive scenarios [39]. The HJB formulation, by contrast, can be solved using standard gradient search algorithms or a more complex damped (Levenberg–Marquardt) method, but only local optimality is guaranteed. To ensure global optimality, a better initial guess is required. The goal of a mixed LP-M/HJB algorithm is to incorporate the advantages of both solution approaches (fast computation, readily available solution techniques, global optimality, and structured on–off solutions) while minimizing the disadvantages (high memory bandwidth and poor performance away from a good initial guess).

The mixed LP-M/HJB algorithm uses the LP technique to construct an initial switch true anomaly set $\boldsymbol{\Theta}_0$ that can be used in a solver in conjunction with the state and costate constraints of the HJB problem to generate an optimal solution. The set $\boldsymbol{\Theta}_0$ gives the true anomalies at which thrusters turn on or off, according to the LP solution. This can be accomplished by restacking the vector $\bar{\boldsymbol{\aleph}}$ into an $m \times M + 2$ matrix:

$$\tilde{\boldsymbol{\aleph}} = [\,\mathbf{0}_{m\times 1} \quad \bar{\boldsymbol{\aleph}}(1{:}m) \quad \bar{\boldsymbol{\aleph}}(m+1{:}2m) \quad \cdots \quad \bar{\boldsymbol{\aleph}}(h-m+1{:}h) \quad \mathbf{0}_{m\times 1}\,] \tag{44}$$

Defining a span of columns of $\tilde{\boldsymbol{\aleph}}$ from the k_1 entry to the k_2 entry as $\tilde{\boldsymbol{\aleph}}_{k_1:k_2}$, the difference across columns is

$$\Delta\tilde{\boldsymbol{\aleph}} = \tilde{\boldsymbol{\aleph}}_{2:M+2} - \tilde{\boldsymbol{\aleph}}_{1:M+1} \tag{45}$$

The matrix $\Delta\tilde{\boldsymbol{\aleph}} \in \mathbb{R}^{m\times M+1}$. The columns of this difference matrix can then be associated with the true anomalies $\{\theta_0, \ldots, \theta_M\}$, and the switching set $\boldsymbol{\Theta}_0$ is given by the elements of $\Delta\tilde{\boldsymbol{\aleph}}$ as follows. The set

$$\boldsymbol{\Theta}_0 = \{\theta_1, \ldots, \theta_m\} \tag{46}$$

where each subset θ_i contains the $n_{p,i}$ pairs of switch true anomalies for the ith thruster. The first element of the jth such pair, $\theta_{i,j-}$, corresponds to the true anomaly associated with the jth instance of 1 in the ith row of matrix $\Delta\tilde{\boldsymbol{\aleph}}$, and the second element corresponds to the jth instance of -1 in the ith row of matrix $\Delta\tilde{\boldsymbol{\aleph}}$. It is important to note that any nonzero elements in a row of $\Delta\tilde{\boldsymbol{\aleph}}$ always occur first as a 1, then as a -1.

The mixed LP-M/HJB algorithm for solving fuel-optimal maneuvers with attitude constraints is presented in Fig. 3; the algorithm is shown with the typical problem parameters, indicating the flexibility that exists in the choice of parameters to achieve a mission objective. This algorithm solves the LP problem using a computationally reasonable discretization M to obtain an initial guess for the HJB

Initialize reference orbit parameters (a, e, μ)
Known: θ_0, θ_F, desired final state $\mathbf{z}(\theta_F)$
Initialize relative orbit parameterization $\mathbf{P}(\theta_0) = [\,p_1, ..., p_6\,]_0$
for each variation in final parameterization $\mathbf{P}(\theta_F) = [\,p_1, ..., p_6\,]_F$
  Define spline integral over $[\,\theta_0, \theta_F\,]$ (Equation 15)
  Solve LP:
    Discretize span $[\,\theta_0, \theta_F\,]$ into M segments
    Construct $\mathcal{Q}_{\mathcal{S}}$ and constraints (Equations 41 and 42)
    Solve Equation 40 with constraints to find $\bar{\aleph}$
  Convert $\bar{\aleph}$ to *on-off* thrusts using tolerance ε (Equation 43)
  Construct initial switching set $\Theta_0 = \{\theta_{1,1-}, \theta_{1,1+}, \cdots, \theta_{m,n_{p,m}-}, \theta_{m,n_{p,m}+}\}$ (Equations 44-46)
  Optimize using HJB Equations 18 and 29 near Θ_0
  Step to next possible final parameterization
end

Fig. 3 Pseudocode for the integrated LP-*M*/HJB for one spacecraft.

solution, which can then be readily calculated to produce near-optimal thrust profiles very quickly.

User-defined variables that affect performance are M, the number of discrete points to solve in the LP initialization; ϵ, the value at which an LP element is considered as a possible thrust point in the HJB initialization; b, the number of iterations allowed for HJB convergence; and δt, the minimum step size allowed in the HJB solver. This step size can be assigned to a value significantly smaller than the discretization step, leading to a more precise on–off solution than would otherwise be available, but also potentially leading to longer convergence times.

D. Benchmark Comparisons of HJB, LP, and Mixed LP-*M*/HJB

To elucidate the differences between HJB, LP, and mixed LP-*M*/HJB, as well as the benefits of the mixed LP-*M*/HJB algorithm, a benchmark problem is defined and simulated. Notationally, the cost associated with a particular method is referred to as $J_F(\cdot)$, where $(\cdot)$ is the method in question. The error in the converted relative reference frame associated with a solution is defined by

$$\Delta|\mathbf{z}_p(\theta_F)| = \left|\begin{bmatrix} 1 & 0 & 0 & 0 & 0 & 0 \\ 0 & 0 & 1 & 0 & 0 & 0 \\ 0 & 0 & 0 & 0 & 1 & 0 \end{bmatrix} \mathbf{z}_{\text{converged}}(\theta_F)\right| - \left|\begin{bmatrix} 1 & 0 & 0 & 0 & 0 & 0 \\ 0 & 0 & 1 & 0 & 0 & 0 \\ 0 & 0 & 0 & 0 & 1 & 0 \end{bmatrix} \mathbf{z}_{\text{desired}}(\theta_F)\right| \tag{47}$$

As noted previously, the general goal of the new algorithm is to incorporate the scalability of the HJB algorithm with the robustness of LP. A good initial guess for converging to a solution that satisfies the HJB equations is generally difficult to obtain, but the LP can provide a good starting point for almost all cases.

Figure 4 shows a comparison of the computation time and performance for the LP and mixed LP-*M*/HJB solvers for a test case of a maneuver in which the spacecraft is rotating at a constant rate of 2 rev/orbit about a reference orbit with perigee distance $a_p \approx$ 7079 km (altitude of 700 km) and eccentricity $e = 0.4$. The spacecraft move from a 12 m radial separation to a 25 m radial separation in one-half of an orbit. Performance can be evaluated in a variety of ways. The left plot compares the computation time of the converged solutions using only linear programming with those obtained using the mixed LP-*M*/HJB. Each vertical line represents a different value of M, as indicated in the figure; the point on the right projects the linear program discretization number M, which requires the same computation time as the mixed technique to solve. The right plot shows the converged precision with respect to the LP-4000/HJB solution, with the projected point indicating the discretization M required for the LP solution to match the precision of the mixed solution. The arrows in the center show whether the extra computation time used by the mixed LP-*M*/HJB algorithm has resulted in a solution with improved precision over LP alone. Upward slanting lines indicate that the precision improves with respect to computation time, and downward slanting lines indicate that the precision decreases for the same computation time. As M increases past 40, the mixed LP-*M*/HJB algorithm quickly obtains a solution that is more precise than LP only for the same computation time. Likewise, as M increases, the computation time for LP-*M*/HJB approaches that of LP-*M*. This illustrates the ability of the mixed LP-*M*/HJB algorithm to resolve solutions more quickly than LP for relatively small discretization number M.

It is notable that the improvements made by the mixed LP-*M*/HJB algorithm are dependent on a good initialization obtained by the LP. In Fig. 5, the scenario is evaluated over a range of eccentricities with perigee distance $a_p \approx 7079$ km, this time with LP initializations of 40, 200, 1000, and 4000. The upper plot shows that the LP technique has difficulty resolving exact solutions for large eccentricities, and the mixed LP-*M*/HJB solution outperforms LP alone in almost all cases. Similarly, as eccentricity increases, for small M, LP fails to approach a solution, which prevents the LP-*M*/HJB technique from obtaining an initial guess; this leads to the failures indicated in the figure. The lower plot illustrates how the final error associated with the rounded LP-*M* solution compares with the error from the LP-*M*/HJB solution: in all cases, the mixed LP-*M*/HJB algorithm converges to a normative pseudoposition $\lesssim 10^{-3}$, but for large e, the rounded LP solution results in a significant errors $\sim 10^3$. This shows that LP has difficulty converging to the bang–off–bang solution structure, achieving instead steadily worsening costs that rely on partial thrusting.

IV. Applications to CU Sat

The Cornell University NanoSat project proposes to place two spacecraft in nearby orbits for the purposes of inspection of one another such that a three-dimensional image of each spacecraft can be reconstructed on the ground [27]. This mission is a demonstration of a variety of autonomous formation technologies, including autonomous formation keeping and maneuvering. The spacecraft will

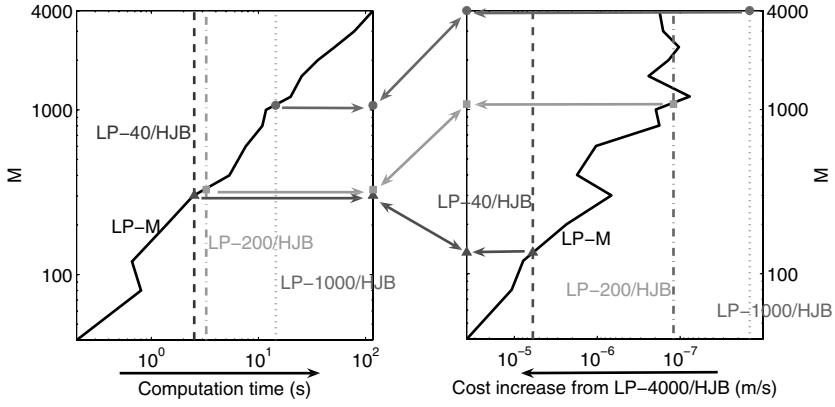

Fig. 4 Comparison of computation time and precision for eccentricity $e = 0.4$ for the test case of 2 rev/orbit rotation rate and perigee distance $a_p \approx 7079$ km (altitude of 700 km).

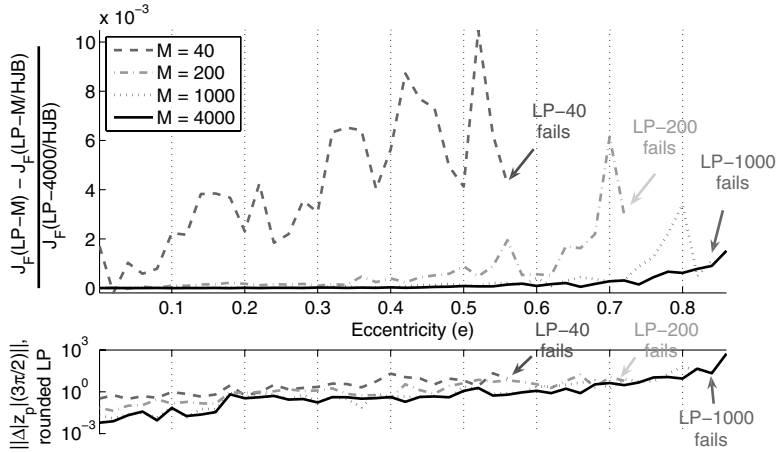

Fig. 5 Difference between LP-*M* converged fuel cost and LP-*M*/HJB converged fuel cost as a function of eccentricity (top) and rounding error incurred by LP for increasing eccentricity (bottom).

reside in low Earth orbit, limiting altitude to a maximum of 1200 km and eccentricity to $e \lesssim 0.1$. The spacecraft are spin-stabilized with a spin rate of near $1^\circ/\text{s}$. Because of the demands of the problem, accounting for thruster rotation is important for planning. Each spacecraft is equipped with eight PPT thrusters capable of producing 60 μN and has a mass of approximately 21 kg.

During the mission, the two spacecraft separate in orbit and must subsequently maneuver into a stable formation before maneuvering again into a position to complete the inspection mission tasks. This section of the paper considers several problems in which one or both spacecraft complete a different maneuver; consideration is given to both single-spacecraft and formation costs, as defined in this paper. The mixed LP-*M*/HJB technique is applied to each of these problems in order to solve for the near-optimal thrust profiles for the sample maneuvers. Because the spacecraft are unlikely to significantly change spin rates during or after maneuvering, each CU Sat spacecraft is assumed to maintain a spin rate of $1^\circ/\text{s}$ through the use of its attitude control system, which is designed to minimize deviations from this nominal rate.

The initial conditions used for computation for all problems in this section are given in the tables in Appendix A. All reconfigurations considered here are performed during the time period $\theta \in [0, (3\pi/2)]$, which allows for error correction in the last quarter of the orbit and ensures that collision-avoidance measures can be employed if necessary. Three simulations are presented. In the first simulation, one spacecraft (*leader*) is taken as the reference center and the other (*follower*) stabilizes its orbit with respect to the reference, resulting in a leader–follower formation. The second example demonstrates a maneuver in which the follower spacecraft moves from leader–follower into a three-dimensional relative orbit such that images can be taken. In the final simulation, a varying reference center location is considered in the formation-maneuver optimization, in which fuel-optimal maneuvers are generated for both spacecraft, with evaluations of both single-spacecraft fuel cost and formation fuel cost. For each example, $M = 800$ is used to adequately capture the problem dynamics without significantly increasing computation time.

A. Entering a Leader–Follower Formation

CU Sat's design indicates that separation will occur normal to the orbital plane; the dynamics of the problem suggest that the resulting orbits will be *unstable* with respect to one another; i.e., the relative path of either spacecraft with respect to the other will not repeat. Before the primary inspection portion of the mission, the CU Sat mission specifies that the spacecraft will move into a leader–follower formation from an unstable formation caused by the initial deployment. A two-stage process is proposed for this maneuver: 1) transiting the desired follower spacecraft into a stable relative orbit (*stabilization*); and 2) transiting from this stable relative orbit into a leader–follower formation (*acquisition*). This two-stage process is appropriate because the instability achieved during separation will make damping of the cross-axis motion before stabilization exceedingly difficult, if not impossible. Initial conditions are chosen to be representative of an orbit-normal separation with a small ($\lesssim$5%) disturbance, and results presented in this paper are typical for such disturbances.

Table 1 shows the initial conditions $p_{(\cdot),0}$ for the unstable relative orbit. Although only one set of initial conditions is shown, simulations over a range of appropriate initial conditions by the authors have yielded similar results. For the two-stage maneuver, there are many degrees of freedom that could be optimized as part of the stabilization portion of the problem. In this example, two parameters are allowed to remain free and the others are constrained: formation-centering parameter $p_{1,\text{st}}$, which is required for any formation that does not undergo relative rotation, and planar displacement parameter $p_{3,\text{st}}$, which captures the relative displacement along the radial direction. The coupling of $p_{2,\text{st}}$ and $p_{3,\text{st}}$ is not necessary, but it simplifies the planar dynamics by damping the motion that is already present, rather than drastically altering it. The stabilized cross-axis parameters $p_{5,\text{st}}$ and $p_{6,\text{st}}$ are selected as the midpoint between the unstable initial condition and the desired leader–follower state, such that thrusts are preferentially selected to complete the primary objective of stabilizing the planar orbit. It is important to note that in this application neither the stabilization or acquisition stage can be completed in a single orbit because of the limited available thrust. Because of this limitation, a final free parameter considered here is given by

$$\mathcal{O} = \frac{\theta_{F,\text{man}} - \theta_0}{2\pi} \tag{48}$$

where $\theta_{F,\text{man}}$ is the first true anomaly after the maneuver is complete such that

$$\theta_{F,\text{man}} \text{mod} 2\pi = \theta_0 \tag{49}$$

The quantity $\mathcal{O}$ defines the number of full orbits over which a stage takes place. For this example, maneuvering during each orbit remains constrained to $\theta \in [0, 3\pi/2]$ such that corrective thrusts can be

Table 1 Parameters for stabilization and acquisition[a]

Parameter	Initial condition ($p_{(\cdot),0}$)	Stabilization ($p_{(\cdot),\text{st}}$)	Acquisition ($p_{(\cdot),\text{ac}}$)
p_1	28.909	$p_{1,\text{st}}$	12.5
p_2	−45.252	$\frac{45.252}{3.5293} p_{3,\text{st}}$	0
p_3	−3.5293	$p_{3,\text{st}}$	0
p_4	−0.90229	0	0
p_5	501.24	501.24/2	0
p_6	−207.62	−207.62/2	0

[a]Reference orbit parameters $\mu = 3.986012 \times 10^{-5}$ km^3/s^2, $a = 7078.931$ km, and $e = 0.04$.

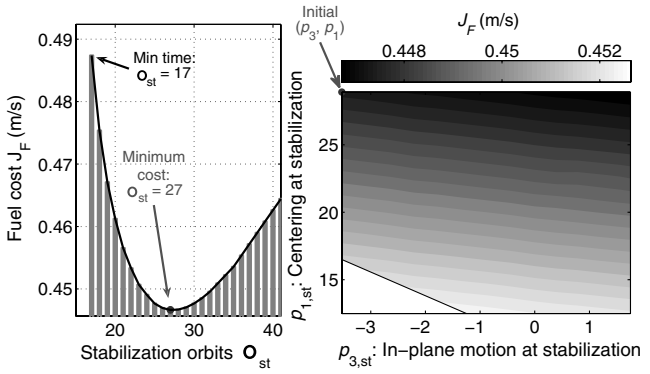

Fig. 6 Minimum fuel cost to stabilize the relative orbit over the allowed parameters ($p_{3,st}$, $p_{1,st}$) for several maneuver lengths $\mathcal{O}_{st}$ (left) and fuel cost to stabilize the relative orbit over the allowed parameters ($p_{3,st}$, $p_{1,st}$) for $\mathcal{O} = 27$ (right).

performed after each orbit; however, such a constraint is not necessary.

It is then clear that the initial acquisition point (the start of the second stage) is identical to the final stabilization point (the end of the first stage), and each stage may be completed over a subset of the total $\mathcal{O}$ number of orbits:

$$\mathcal{O} = \mathcal{O}_{st} + \mathcal{O}_{ac} \tag{50}$$

After the completion of any full orbit in which the final parameterization is unstable, the parameterization must be recalculated for true anomaly $\theta \in [0, 2\pi]$ to ensure that drift is accounted for. Note that no such reparameterization is required for full orbits that result in a stable parameterization, as stable parameterizations are invariant with true anomaly. The objective in this section is to determine the optimal maneuvering strategy to successfully (and safely) complete the two-stage scenario.

For this simulation, the desired final parameterization after both stages places the spacecraft 13 m apart at true anomaly $\theta = \pi$; note that this corresponds to $p_1 \approx 12.5$. The optimization then probes the allowed intermediate stage parameters ($p_{1,st}$, $p_{3,st}$) that minimize the required fuel. It necessarily does not consider any value of $p_{1,st}$ or $p_{3,st}$ that may endanger the spacecraft. In particular, the problem formulation assumes that the spacecraft should not move within 10 m of one another at any point in their respective orbits or during maneuvering, once stabilization has been achieved. By constraining the parameters ($p_{5,st}$, $p_{6,st}$) to be those given in Table 1, and by further constraining the centering parameter be in the range $p_{1,0} = 28.5 \leq p_{1,st} \leq 12.5 \approx p_{1,ac}$, this prevents the interspacecraft distance from exceeding 10 m by constraining $p_{3,st} \lesssim 1.75$.

To understand the sensitivities associated with the stabilization (first) stage alone, a multistage mission optimization is defined as

$$\min_{\mathcal{O}_{st}} \left[\min_{(p_{3,st}, p_{1,st})} \quad J_{F,st} \right] \tag{51}$$

Figure 6 compares the fuel cost computed using Eq. (21) for the stabilization stage over the allowed optimization parameter space ($p_{3,st}$, $p_{1,st}$) for multistep maneuvers requiring $\mathcal{O}_{st} \in [17, 42]$. Given a defined $\mathcal{O}_{st}$, the minimum cost occurs at the stabilization point $(p_{3,st}, p_{1,st}) = (p_{3,max}, p_{1,0})$. A global minimum fuel cost occurs for $\mathcal{O}_{st,min} = 27$. Preserving the formation center $p_{1,0}$ simply minimizes the energy required to change the orbit. Likewise, forcing an increase in $p_{3,st}$ reduces the relative planar drift across successive orbits; this allows successive maneuvers to better force $p_{4,st} \to 0$ by reducing orbit-to-orbit variations in this parameter. However, such variations depend on the maneuver being sufficiently short, such that the drift associated with the instability does not dominate the stabilization thrust. Additionally, this scenario shows that changes to along-track p_1 are more costly than variations in radial p_3, particularly when performed in conjunction with stabilization near the minimum final true anomaly.

The acquisition stage begins at the stabilization point and ends with a leader–follower formation with $p_{1,ac} = 12.5$ and $p_{i,ac} = 0$ for $i \in \{2, \ldots, 6\}$; this parameterization results in the desired minimum separation of 13 m between the spacecraft at true anomaly $\theta = \pi$. This problem is cast similar to the prior example as the multistage optimization of

$$\min_{\mathcal{O}_{ac}} \left[\min_{(p_{1,st}, p_{3,st})} \quad J_{F,ac} \right] \tag{52}$$

Figure 7 shows the fuel cost as a function of the stabilization parameters ($p_{1,st}$, $p_{3,st}$) for four maneuver lengths ($\mathcal{O}_{ac} \in \{16, 18, 20, 22\}$) for the acquisition stage. The minimum in this set requires the most orbits to complete, with $\mathcal{O}_{ac}$ largely determining the stage fuel use. However, as the allowed number of orbits increases, the fuel cost of varying $p_{3,st}$ becomes a less important factor in determining the minimum-fuel solution, a result of the longer maneuver time allowing relative motion to be more slowly damped for the same amount of fuel. For increased $\mathcal{O}_{ac}$, the absolute cost then decreases significantly.

The leader–follower formation problem is now considered as an optimization over both stages, stabilization and acquisition. This is defined by

$$\min_{\mathcal{O}} [\min_{(p_{1,st}, p_{3,st})} \quad J_F], \qquad \mathcal{O} = \mathcal{O}_{st} + \mathcal{O}_{ac} \tag{53}$$

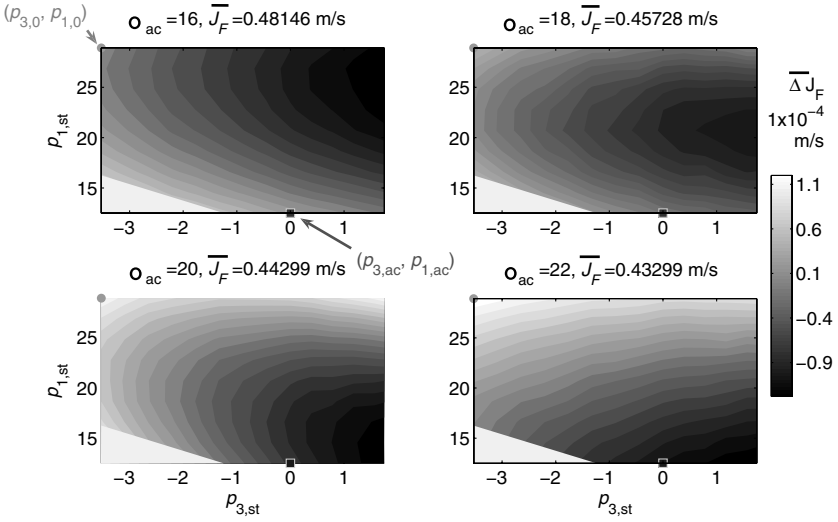

Fig. 7 Comparative cost to perform the acquisition stage of the maneuver as a function of stabilization parameters $p_{1,st}$ and $p_{3,st}$ for increasing number of allowed orbits $\mathcal{O}_{ac}$.

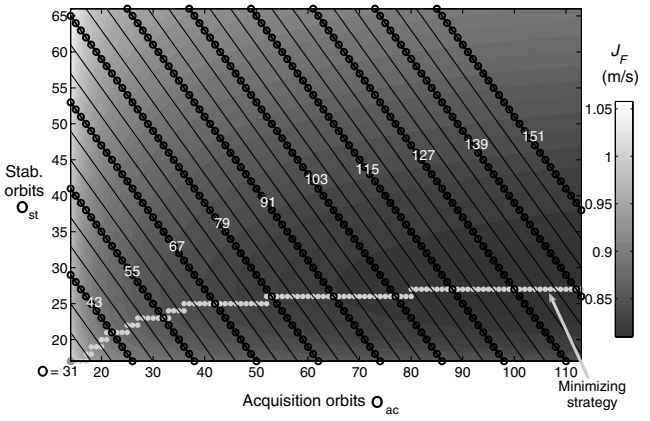

Fig. 8 Minimum fuel cost to perform both the stabilization and acquisition stages of the maneuver to establish a leader–follower formation as it varies with orbit numbers $\mathcal{O}_{st}$ and $\mathcal{O}_{ac}$.

Figure 8 gives the minimum fuel cost over the range of allowed optimization parameters for different maneuver lengths $\mathcal{O}$, separated into the stabilization-stage length $\mathcal{O}_{st}$ and acquisition-stage length $\mathcal{O}_{ac}$. Diagonal lines and open dots indicate fixed maneuver lengths $\mathcal{O} = \mathcal{O}_{st} + \mathcal{O}_{ac}$. The minimum cost for each $\mathcal{O}$ is indicated by a solid dot. For small $\mathcal{O}$, the optimal strategy is to enforce as short a stabilization stage as possible, as the fuel savings achieved by slightly increasing $\mathcal{O}_{st}$ are significantly less than those achieved by corresponding increases in $\mathcal{O}_{ac}$. For longer maneuver times $\mathcal{O}$, this strategy is supplanted by one in which the stabilization stage is performed near its fuel-optimal number of orbits $\mathcal{O}_{st}$ while the stabilization occupies the remaining allowed maneuver period. These results also indicate that a longer maneuver time can result in a significant fuel savings only if most of the additional orbits are devoted to acquisition. The minimum for all orbit numbers is achieved for stabilization parameterization $(p_{1,st}, p_{3,st}) = (p_{1,0}, 1.75)$. This is a byproduct of the strong dependence of the stabilization fuel cost and weak dependence of the acquisition fuel cost on stabilization parameterization. In addition, although a larger $p_{3,st}$ does provide for a smaller fuel cost, the resultant formation does not provide adequate safety margins for spacecraft separation.

B. Initiating Relative Motion About Each Spacecraft: Single-Spacecraft Maneuver

With the spacecraft established in a stable leader–follower formation, the mission objectives can be achieved only through additional maneuvering. In particular, the two spacecraft must take up motions relative to each other in order to generate a useful set of photographs for inspection. Again, the scenario considered here fixes one spacecraft (leader) while allowing the other (follower) to move into a stable relative orbit centered around the leader. Because the maneuver is small, this transit can be performed in a single orbit. The optimization must constrain $p_1 = 0$ to create a centered orbit, as required for inspection. To simplify this formation optimization problem, two additional constraints are employed, as shown in Table 2: a separation of 12 m is achieved at true anomaly $\theta_C = \pi$ and $\dot{x}_3^R(\theta_C) = 0$. The desired final position then resides on a 12 m sphere about the leader at the critical true anomaly $\theta = \theta_C$. The choice of θ_C in this case allows the spacecraft to maneuver to the desired point as it approaches apogee, where slow orbital dynamics will allow for viewing and photographing over a range of true anomalies about $\theta = \pi$ with little variation in separation distance.

Table 2 Constraint parameters for initiating relative motion from a leader–follower formation[a]

Constraint parameter	Leader–follower $(p_{(\cdot),lf})$	Relative motion $(p_{(\cdot),sph})$
p_1	12.5	0
p_4	0	0
θ_C	π	π
$\dot{x}_3^R$	0	0
ϕ	0	ϕ_{sph}
ν	0	ν_{sph}

[a]Reference orbit parameters $\mu = 3.986012 \times 10^{-5}$ km^3/s^2, $a = 7078.931$ km, and $e = 0.04$.

The final formation parameterization is now defined for the optimization problem. Defining the vector connecting the leader to the follower as $\Delta\mathbf{x}^R = \mathbf{x}^R_{foll} - \mathbf{x}^R_{lead}$, the constraint that the relative distance between the spacecraft lie on a sphere is given by $\|\Delta\mathbf{x}^R\| = \varrho$, where ϱ is the separation distance. This condition constrains the vector $\Delta\mathbf{x}^R$ to a sphere centered about the leader spacecraft. Positions on this sphere can be defined in spherical coordinates via an azimuthal angle ϕ measured from the against-track vector for the reference leader spacecraft, $\hat{x}_1^R$, and an elevation angle ν measured from a plane parallel to the plane containing unit vectors $\hat{x}_1^R$ and $\hat{x}_2^R$, in which the leader spacecraft resides, at height $x^R_{3,lead}$. The Cartesian coordinate analogues for the elements of $\Delta\mathbf{x}^R$ are

$$\Delta x_1^R = \varrho \cos\phi \cos\nu \tag{54}$$

$$\Delta x_2^R = \varrho \sin\phi \cos\nu \tag{55}$$

$$\Delta x_3^R = \varrho \sin\nu \tag{56}$$

The optimization problem addressed by this example is then given as

$$\min_{(\phi,\nu)} J_F \tag{57}$$

Figure 9 shows the cost to maneuver to the set of possible final angles ϕ_{sph} and ν_{sph} from a 13 m leader–follower formation at critical true anomaly $\theta_C = \pi$ to a relative orbit in which the leader spacecraft resides at the origin and the follower spacecraft has $\varrho = 12$ m at $\theta_C = \pi$. The three-dimensional surface this creates is also shown.

This optimization problem results in cost contours with multiple local minima. The global minimum occurs for a final parameterization in which the spacecraft is at $\nu_{sph} \approx 8°$ and $\phi_{sph} \approx 0°$ at $\theta = \theta_C$. At this location, the cross-axis variation is small and the change in parameter p_3 is minimized. Because inclination changes are generally costly, the low cost associated with limiting such cross-axis motion is reasonable. The slight elevation associated with this minimum is due to the thruster placements and body rotation; for a nonrotating spacecraft with axial thrusters, the fuel cost would be symmetric about $\nu = 0$. The maximum is for the spacecraft to transition to $\phi_{sph} \approx 135°$ (approximately azimuthally normal to the minimum) with a small cross-axis displacement. In this region, the fuel required to increase p_3 to meet the problem constraints is more significant than the general cost increase associated with a variation in cross-axis parameters. This example demonstrates the importance for spacecraft designers to consider the possible effects of thruster placements in addition to other factors during each phase of the mission, and it illustrates how the theory developed in this paper can be used in conjunction with the spacecraft design process to motivate both thruster placements and formation selection.

C. Initiating Two-Spacecraft Relative Motion

Because both spacecraft in the CU Sat formation are identical, allowing one spacecraft to perform all maneuvers does not make efficient use of the available resources. To reduce the burden on each spacecraft, maneuvers should be considered in context of mission objectives and mission lifetime, which typically require fuel expenditure from both spacecraft. This example considers the maneuver in which the spacecraft move from leader–follower to a relative motion about one another, similar to the example in Sec. IV.B, with alternative formation centers.

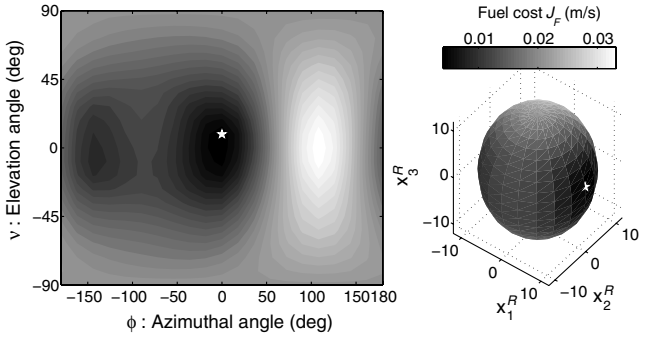

Fig. 9 Fuel cost for moving from a leader–follower formation to distance $\varrho = 12$ m at $\theta_C = \pi$.

The selection of a global formation center can have significant effects on the use of resources in a cluster of spacecraft, including fuel, computational effort, and communication bandwidth. The CU Sat mission will use a carrier-phase differential Global Positioning System (GPS) to determine relative position and velocity to millimeter accuracy [40]; thus, with the absolute orbital data from either spacecraft with respect to the Earth, the formation center can be defined anywhere along a line connecting the spacecraft. For large formations, a complex scheme must often be used to determine the formation center [41]. However, the CU Sat pair can take advantage of the carrier-phase differential GPS capabilities and assign the formation center between the two spacecraft at a fractional distance, greatly simplifying the formation-center selection problem.

Similar to the single-spacecraft maneuver in the previous subsection, constraints of a 12 m separation at $\theta_C = \pi$ and $\dot{x}_3^R(\theta_C) = 0$ are imposed. An additional third constraint is added to this problem that enforces that each spacecraft resides at the endpoint of a 12 m line passing through the reference center at true anomaly $\theta = \theta_C$. This center is defined by the fraction v and positions in the inertial frame as

$$\mathbf{R} = v\mathbf{R}_{\text{foll}} + (1 - v)\mathbf{R}_{\text{lead}} \tag{58}$$

This section examines the effect of varying v on the cost to the spacecraft individually as well as the cost to the formation as a whole.

The full optimization problem for the mission is given as

$$\min_{v}\left[\min_{(\phi,\nu)} J_{F,\text{lead}}(v,\phi,\nu) + J_{F,\text{foll}}(v,\phi,\nu)\right] \tag{59}$$

The multistage optimization can then be extended to optimizing over v, the formation-center location. In general, increasing v has little effect on the location of the fuel-optimal final relative locations of the spacecraft at true anomaly $\theta = \pi$. The optimal strategy always places the follower spacecraft near azimuthal angle $\phi \approx 0°$ and elevation angle $\nu \approx 8°$. Slight variations appear in these values as v varies due to the differences in rotations between the two spacecraft.

Although the angles describing the fuel-optimal parameterizations of the two spacecraft with respect to one another do not vary significantly with v, the value of that minimum does change, as shown in the upper portion of Fig. 10. The formation fuel use for this maneuver (defined as the sum of the fuel used by the two spacecraft in completing the maneuver) achieves a minimum when the spacecraft partition the work equally between one another, which leads to a fuel savings of approximately 8% for the formation. This point is marked with a star in the figure. It is notable, however, that the cost borne by the leader spacecraft varies almost linearly with v; in situations in which absolute fuel use or fraction of total fuel use by only one member of the formation pair is the primary consideration, the optimal maneuvering strategy for both formation members can be quickly established. Similar fuel-saving results occur in the formation-keeping problem if both spacecraft are tasked to transit during the maneuvers. The method and results presented here will allow such flexibility to be used on CU Sat-like missions to maximize resource potential in achieving objectives.

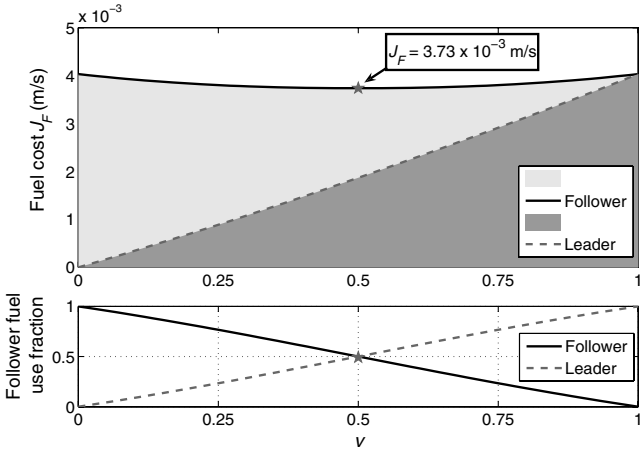

Fig. 10 Total minimum formation fuel cost, partitioned by spacecraft (top) and fractional fuel use by leader spacecraft (bottom).

V. Conclusions

A novel algorithm for solving general formation minimum-fuel problems with attitude dynamics in a relative reference frame using linear programming in conjunction with Hamilton–Jacobi–Bellman optimality conditions has been presented. The method scales better computationally than LP while providing the solution guarantees of a numerical HJB solution. The mixed LP-*M*/HJB algorithm can be used to solve a variety of complex problems in which HJB constraints are known but no initial guess is available. Because the method does not rely on discretization of the dynamics, it efficiently uses memory and processor time and scales well with important system parameters, such as eccentricity and number of orbits.

The mixed LP-*M*/HJB method is applied here to the particular problem of a spacecraft formation that operates in a realistic space environment with known attitude dynamics. These dynamics were then used in conjunction with the combined LP-*M*/HJB algorithm to solve several examples involving the Cornell University NanoSat project. Optimal formation maneuvers have been generated for modes that take the spacecraft from initial separation to stable relative orbits and data-taking. Different formation centers were also considered, including the cost to both the formation and the individual spacecraft. Such information will be useful to CU Sat operators and those designing missions with similar goals. It will provide a single tool for prelaunch analysis of strategies in the context of mission objectives and mission life, as well as for on-orbit decision-making for achieving specific mission objectives.

Appendix A: Simulation Data

Initial conditions for the CU Sat spacecraft for the example simulations are provided in Table A1 as a reference. Separation conditions are the values used at the instant of separation for an

Table A1 Separation conditions for CU Sat example

Global $(x_1^N, \dot{x}_1^N, x_2^N, \dot{x}_2^N, x_3^N, \dot{x}_3^N)^T$	Orbital elements $(a, e, i, \omega, \Omega, \theta)^T$
Spacecraft 1 (leader)	
$3.46869135464401 \times 10^3$ km	7078.93100 km
−6.52398592580395 km/s	0.04000000
$4.75600512902940 \times 10^3$ km	42.3000000°
2.37242325309425 km/s	14.0000000°
$3.43551261223094 \times 10^3$ km	26.0000000°
3.53075327556610 km/s	22.5000000°
Spacecraft 2 (follower)	
$3.46869135464401 \times 10^3$ km	7078.93342 km
−6.52388735457831 km/s	0.04000051
$4.75600512902940 \times 10^3$ km	42.3029145°
2.37203625321527 km/s	14.0048943°
$3.43551261223094 \times 10^3$ km	25.9957822°
3.53119812624019 km/s	22.5005979°

Table A2 Thrust vectors in body coordinates (thrust to mass $u = 60/21 \times 10^{-6}$ m/s^2)

−0.6124	0.6124	−0.6124	0.6124	−0.6124	0.6124	−0.6124	0.6124
0.3536	−0.3536	0.3536	−0.3536	−0.3536	0.3536	−0.3536	0.3536
−0.7071	0.7071	0.7071	−0.7071	−0.7071	0.7071	0.7071	−0.7071

impulsive change in velocity; the positions of the spacecraft are identical. Thruster positions for the two spacecraft are as shown in Table A2. Rotation occurs in the quaternion sense about a different vector for each spacecraft. For quaternion

$$\mathbf{q} = [\sin(\zeta/2)\mathbf{a}, \cos(\zeta/2)]^T$$

where ζ is the angle of rotation about the vector $\mathbf{a}$,

$$\mathbf{a}_{s/c,1} = \begin{pmatrix} 0.2575 \\ 0.0536 \\ 0.9648 \end{pmatrix}, \qquad \mathbf{a}_{s/c,2} = \begin{pmatrix} 0.0990 \\ 0.0990 \\ 0.9901 \end{pmatrix} \tag{A1}$$

References

[1] "Solving Magnetospheric Acceleration, Reconnection, and Turbulence (SMART)," NASA AO 03-OSS-01, 2004.

[2] "The Magnetospheric Constellation Mission Dynamic Response and Coupling Observatory (DRACO): Understanding the Global Dynamics of a Structured Magnetotail," NASA TM 2001209985, May 2001.

[3] Tsien, W. P., Finley, C., Mocio, M., and Olmedo, C., "Advancing Military-Relevant Space Technologies," *AIAA Space 2003 Conference Proceedings*, Vol. 2, AIAA, Reston, VA, 2003, pp. 1013–1025; also AIAA Paper 2003-6363.

[4] Gendreau, K. C., Cash, W. C., Shipley, A. F., and White, N., "MAXIM Pathfinder X-Ray Interferometry Mission," *Proceedings of SPIE: The International Society for Optical Engineering*, Vol. 4851, March 2003, pp. 353–364. doi:10.1117/12.461316

[5] Tillerson, M., and How, J. P., "Advanced Guidance Algorithms for Spacecraft Formation-Keeping," *Proceedings of the American Control Conference*, Vol. 4, Inst. of Electrical and Electronics Engineers, Piscataway, NJ, 2002, pp. 2830–2835.

[6] Wertz, J. R., and Bell, R., "Autonomous Rendezvous and Docking Technologies—Status and Prospects," *Proceedings of SPIE: The International Society for Optical Engineering*, Vol. 5088, 2003, pp. 20–30.

[7] Scharf, D. P., Hadeagh, F. Y., and Ploen, S. R., "A Survey of Spacecraft Formation Flying Guidance and Control (Part 1): Guidance," *Proceedings of the American Control Conference*, Inst. of Electrical and Electronics Engineers, Piscataway, NJ, June 2003, pp. 1733–1739.

[8] Sabol, C., Burns, R., and McLaughlin, C. A., "Satellite Formation Flying Design and Evolution," *Journal of Spacecraft and Rockets*, Vol. 38, No. 2, 2001, pp. 270–278. doi:10.2514/2.3681

[9] Kumar, R., and Seywald, H., "Fuel-Optimal Stationkeeping Via Differential Inclusions," *Journal of Guidance, Control, and Dynamics*, Vol. 18, No. 5, 1995, pp. 1156–1162. doi:10.2514/3.21519

[10] Guibot, V. M., and Scheeres, D. J., "Solving Relative Two-Point Boundary Value Problems: Spacecraft Formation Flight Transfer Application," *Journal of Guidance, Control, and Dynamics*, Vol. 27, No. 4, July–Aug. 2004, pp. 693–704. doi:10.2514/1.11164

[11] Eades, J. B., Jr., "Operational Requirements and the Geometry of a Station-Keeping Maneuver," *Celestial Mechanics*, Vol. 16, Nov. 1977, pp. 315–342. doi:10.1007/BF01232658

[12] Tillerson, M., Inalhan, G., and How, J. P., "Coordination and Control of Distributed Spacecraft Systems Using Convex Optimization Techniques," *International Journal of Robust and Nonlinear Control*, Vol. 12, Nos. 2–3, 2002, pp. 207–242. doi:10.1002/rnc.683

[13] Zanon, D. J., and Campbell, M. E., "Fuel Optimal Maneuvers with Spacecraft Attitude Constraints," *Proceedings of the AIAA Guidance, Navigation, and Control Conference*, AIAA, Reston, VA, Aug. 2006, pp. 4129–4144; also AIAA Paper 2006-6588.

[14] Zanon, D. J., and Campbell, M. E., "Optimal Planner for Spacecraft Formations in Elliptical Orbits," *Journal of Guidance, Control, and Dynamics*, Vol. 29, No. 1, Jan.–Feb. 2006, pp. 161–171. doi:10.2514/1.7236

[15] Beard, R. W., and Hadeagh, F. Y., "Finite Thrust Control for Satellite Formation Flying with State Constraints," *Proceedings of the American Control Conference*, Inst. of Electrical and Electronics Engineers, Piscataway, NJ, 1999, pp. 4383–4387.

[16] Shaohua, Y., "Autonomous rendezvous in elliptical orbits," *Acta Astronautica*, Vol. 41, No. 2, July 1997, pp. 95–101. doi:10.1016/S0094-5765(97)00204-X

[17] Garcia, I., and How, J. P., "Trajectory Optimization for Satellite Reconfiguration Maneuvers with Position and Attitude Constraints," *Proceedings of the 2005 American Controls Conference*, Vol. 2, Inst. of Electrical and Electronics Engineers, Piscataway, NJ, 2005, pp. 889–894.

[18] Beard, R. W., and Hadeagh, F. Y., "A Coordination Architecture for Spacecraft Formation Control," *IEEE Transactions on Control Systems Technology*, Vol. 9, No. 6, 2001, pp. 777–790.

[19] Hall, C. D., and Ross, I. M., "Optimal Attitude Control for Coplanar Orbit Phasing Transfers," *Advances in the Astronautical Sciences*, Vol. 115, 2003, pp. 79–94; also American Astronautical Society, Paper 03-262.

[20] Tietz, J. C., and Almand, B. J., "Autonomous Spacecraft Rendezvous and Docking," *Proceedings of the Eighth Annual Rocky Mountain Conference on Guidance and Control*, Univelt, San Diego, CA, 1985, pp. 191–198.

[21] Hablani, H. B., Tapper, M. L., and Dana-Bashian, D. J., "Guidance and Relative Navigation for Autonomous Rendezvous in a Circular Orbit," *Journal of Guidance, Control, and Dynamics*, Vol. 25, No. 3, May–June 2002, pp. 553–562. doi:10.2514/2.4916

[22] Zimpfer, D., Kachmar, P., and Tuohy, S., "Autonomous Rendezvous, Capture and In-Space Assembly: Past, Present and Future," *AIAA 1st Space Exploration Conference*, AIAA, Reston, VA, 2005, pp. 234–245; also AIAA Paper 2005-2523.

[23] Machula, M. F., and Gandhoo, G. S., "Rendezvous and Docking for Space Exploration," *AIAA 1st Space Exploration Conference*, AIAA, Reston, VA, 2005, pp. 1–10; also AIAA Paper 2005-2716.

[24] Polites, M. E., "Technology of Automated Rendezvous and Capture in Space," *Journal of Spacecraft and Rockets*, Vol. 36, No. 2, Mar–Apr 1999, pp. 280–291. doi:10.2514/2.3443

[25] Guerra, C. J., and Page, L. A., "Autonomous Planning for Satellite Rendezvous and Proximity Operations," *In-fotech@Aerospoace*, AIAA, Reston, VA, 26–29 Sept. 2005, pp. 1–13; also AIAA Paper 2005-7026.

[26] Breger, L., and How, J. P., "Safe Trajectories for Autonomous Rendezvous of Spacecraft," *Journal of Guidance, Control, and Dynamics*, Vol. 31, No. 5, 2008, pp. 1478–1489. doi:10.2514/1.29590

[27] Peck, M. A., *CUSat: An End-to-End In-Orbit Inspection System University Nanosatellite Program*, U.S. Dept. of Defense Rept. A764574, 2007.

[28] Kornfeld, R. P., Bunker, R. L., Cucullu, G. C., Essmiller, J. C., Hadaegh, F. Y., Liebe, C. C., Padgett, C. W., Wong, E. C., Seereeram, S., and Mehra, R. K., "New Millennium ST6 Autonomous Rendezvous Experiment (ARX)," *Proceedings of the IEEE Aerospace Conference*, Vol. 1, Inst. of Electrical and Electronics Engineers, Piscataway, NJ, 2003, pp. 368–380.

[29] Inalhan, G., Tillerson, M., and How, J. P., "Relative Dynamics and Control of Spacecraft Formations in Eccentric Orbits," *Journal of Guidance, Control, and Dynamics*, Vol. 25, No. 1, 2002, pp. 48–59. doi:10.2514/2.4874

[30] Tschauner, J., and Hempel, P., "Rendezvous zu Einem in Elliptischer Bahn Umlaufenden Ziel," *Astronautica Acta*, Vol. 11, No. 5, 1965, pp. 104–109.

[31] Humi, M., "Fuel-Optimal Rendezvous in a General Central Force Field," *Journal of Guidance, Control, and Dynamics*, Vol. 16, No. 1, 1993, pp. 215–216. doi:10.2514/3.11448

[32] Carter, T. E., "State Transition Matrices for Terminal Rendezvous Studies: Brief Survey and New Example," *Journal of Guidance,*

Control, and Dynamics, Vol. 21, No. 1, 1998, pp. 148–155. doi:10.2514/2.4211

[33] de Boor, C., *A Practical Guide to Splines*, Springer–Verlag, New York, 1978.

[34] Farin, G., *NURBS: From Projective Geometry to Practical Use*, A. K. Peters, Natick, MA, 1999.

[35] Campbell, M. E., and Schetter, T., "Comparison of MultiAgent Based Organizations for Satellite Constellations," *Journal of Spacecraft and Rockets*, Vol. 39, No. 2, March–April 2002, pp. 274–283. doi:10.2514/2.3809

[36] Rayburn, C. D., Campbell, M. E., and Mattick, A. T., "Pulsed Plasma Thruster System for Microsatellites," *Journal of Spacecraft and Rockets*, Vol. 42, No. 1, Jan.–Feb. 2005, pp. 161–170. doi:10.2514/1.15422

[37] Campbell, M. E., "Planning Algorithm for Multiple Satellite Clusters," *Journal of Guidance, Control, and Dynamics*, Vol. 26, No. 5, 2003, pp. 770–780. doi:10.2514/2.5111

[38] Hoffman, H. J., and Wielandt, H. W., "The Variation of the Spectrum of a Normal Matrix," *Duke Mathematical Journal*, Vol. 20, 1953, pp. 37–39.

[39] Kall, P., and Mayer, J., *Stochastic Linear Programming: Models, Theory, and Computation*, Springer Science and Business Media, New York, 2005.

[40] Leung, S., and Montenbruck, O., "Real-Time Navigation of Formation-Flying Spacecraft Using Global-Positioning-System Measurements," *Journal of Guidance, Control, and Dynamics*, Vol. 28, No. 2, March–April 2005, pp. 226–235. doi:10.2514/1.7474

[41] Tillerson, M., Breger, L., and How, J. P., "Distributed Coordination and Control of Formation Flying Spacecraft," *Proceedings of the IEEE American Control Conference*, Inst. of Electrical and Electronics Engineers, Piscataway, NJ, 2003, pp. 1740–1745.

C. McLaughlin
Associate Editor